Lanthanide-doped inorganic nanoparticles turn molecular triplet excitons bright

Sanyang Han[1#], Renren Deng[1,2#*], Qifei Gu[1], Limeng Ni[1], Uyen Huynh[1], Jiangbin Zhang[1,3], Zhigao Yi[4], Hiroyuki Tamura[5], Anton Pershin[6], Hui Xu[7], Mojtaba Abdi-Jalebi[1], Aditya Sadhanala[1], Artem Bakulin[3], David Beljonne[6], Xiaogang Liu[4*] and Akshay Rao[1*]

[1]Cavendish Laboratory, University of Cambridge, Cambridge CB3 0HE, United Kingdom.
[2]State Key Laboratory of Silicon Materials, School of Materials Science and Engineering, Zhejiang University, Hangzhou 310027, China.
[3]Department of Chemistry, Imperial College London, London SW7 2AZ, United Kingdom.
[4]Department of Chemistry, National University of Singapore, Singapore 117543, Singapore.
[5]Department of Chemical System Engineering, The University of Tokyo, Tokyo, 113-8656, Japan.
[6]Laboratory for Chemistry of Novel Materials, University of Mons, Place du Parc 20, B-7000, Mons, Belgium.
[7]School of Chemistry and Material Science, Heilongjiang University, Harbin 150080, China.

[#]These authors contributed equally to this work.

*Correspondence author. Email: ar525@cam.ac.uk (A.R.), chmlx@nus.edu.sg (X.L.), rdeng@zju.edu.cn (R.D.)

One sentence summary: Spin exchange and charge transfer interactions between molecules and lanthanide-doped nanoparticles allow for unprecedented control of dark triplet excitons.

Abstract: The generation, control and transfer of triplet excitons in molecular and hybrid systems is of great interest for applications such as light emission, photon frequency conversion and photocatalysis. Triplet dynamics are generally controlled through heavy-metal based spin-orbit coupling or singlet-triplet energy splitting. Here we demonstrate that it is possible to control triplet dynamics by coupling organic molecules to lanthanide-doped inorganic nanoparticles through spin-exchange and charge-transfer interactions. This coupling enables direct photogeneration of triplet excitons from the ground state, radiative harvesting of triplet excitons, and an unprecedented lanthanide-triplet exciton fusion process that gives highly efficient upconversion. These results provide a new paradigm to control triplet excitons, a capability that is essential for many fields of research such as photocatalysis, optoelectronics, photodynamic therapy, and photon frequency conversion.

Spin-1 triplet excitons can exhibit long lifetimes and diffusion length in both solid-state and solution phase systems, allowing them to act as energy carriers over long distances in optoelectronic applications, such as light emission and photon upconversion, as well as serving as energy reservoirs for photocatalytic applications (*1-6*). However, a fundamental limitation of using molecular triplet excitons is that they are 'dark states' and must be produced from the photogenerated singlet state via intersystem-crossing, as the direct optical excitation of the spin-1 triplet exciton from the spin-0 singlet ground state is forbidden and similarly their radiative return to the ground state is forbidden (*7-9*). Conventionally, the efficient generation of triplets has been limited to molecules with intramolecular heavy metal complexing or special halogen and deuterated carbon scaffolds (*10-12*). Similarly, the luminescent harvesting of triplets requires heavy-metal complexing or the engineering of molecules with small singlet-triplet energy splitting. This constraint places strict criteria on the design of molecular systems that uses triplet excitons. Here, we demonstrate that conventional molecular systems can be efficiently coupled to lanthanide-doped inorganic nanocrystals via spin-exchange and charge-transfer (CT) interactions. This allows for the direct photogeneration of triplets from the ground state, radiative harvesting of triplets via transfer to the lanthanide nanoparticle followed by emission, and a new lanthanide-triplet exciton fusion process that gives highly efficient upconversion. Our results establish a new and highly tuneable platform for the creation of 'bright' and long-lived triplet excitons and the transfer and manipulation of their energy, thus opening up new avenues for optoelectronics, photosensitization, photocatalysis, sensing, light emission, lasing and photon frequency conversion.

Figure 1A shows a schematic of a lanthanide-doped nanocrystal ($NaLnF_4$) and the structures of the model molecules used in our study (tetracene, rubrene and 9-[3-carboxyl-4-(diphenylphosphinoyl)phenyl]-9H-carbazole (CPPOA)), along with their triplet energies. $NaLnF_4$ is an

insulating host and the doped lanthanide ions are the only electronically active component. We prepared blended films of organic molecules and $NaGdF_4$:50%Yb nanocrystals by drop-casting (figs. S1 and S2). The blend film ensures that organic molecules are in close contact with the lanthanide ions at or near the surface of the nanoparticles (See SM for structural characterization). Yb^{3+} was chosen as the energy gap between the lowest excited state ($^2F_{5/2}$), and the ground state ($^2F_{7/2}$) of Yb^{3+} is 1.25 eV (fig. S3), and hence lies between the triplet energy levels of tetracene (1.25 eV; ref *13*) and rubrene (1.14 eV; ref *14*).

Figure 1B shows the absorption spectra, measured by photothermal deflection spectroscopy (PDS), of a $NaGdF_4$:Yb-rubrene blend film, a pristine rubrene film and a film of the only $NaGdF_4$:Yb. Apart from the normal absorption features associated with the $S_0 \rightarrow S_n$ transitions in rubrene, we observe new absorption features between 700-1100 nm in the $NaGdF_4$:Yb-rubrene blend film. In contrast, the pristine rubrene film has no absorption in the same region, while the $NaGdF_4$:Yb film shows only a narrow Yb^{3+} absorption between 900-1050 nm. Significantly, the PDS spectra reveal a ~ 500 fold enhancement in the near-infrared (NIR) absorbance of the $NaGdF_4$:Yb-rubrene blend compared with the pristine rubrene film. To understand this observation, we performed Density Functional Theory (DFT) calculations combined with the multireference second-order Møller-Plesset perturbation theory (MRMP2) (See SM for details). We found that the experimentally measured absorption in the NIR region matches well with the calculated absorption for the $S_0 \rightarrow T_n$ transition for an isolated rubrene molecule based on a simple displaced harmonic oscillator model, as shown in Figure 1C. Note that theoretical prediction for the 0-0 transition shows a much higher intensity. We attributed this suppression of the 0-0 band to a Herzberg-Teller (HT) mechanism, as has been described previously (*15*). The extra absorption in the $NaGdF_4$:Yb-rubrene blend film is thus assigned to the $S_0 \rightarrow T_n$ transition

of rubrene, implying that the usually dark $S_0 \rightarrow T_n$ transition has become bright in the blend. Similarly, we also observed a significant increase in sub-gap absorption in the blends of $NaGdF_4$:Yb with tetracene, which is consistent with the expected $S_0 \rightarrow T_n$ transitions (fig. S4).

These data show that in the presence of the $NaGdF_4$:Yb nanoparticles, the direct $S_0 \rightarrow T_n$ transitions gain significant oscillator strength. One explanation for this could be related to spin-orbit coupling associated with the presence of the heavy atoms (Z = 70 for Yb). To test this hypothesis, blends of rubrene were made with $NaGdF_4$, $NaYF_4$ and $NaLuF_4$ nanocrystals. Gd^{3+} (Z = 64) has seven unpaired 4f electrons with a total spin of eight[4], while Y^{3+} (Z = 39) and Lu^{3+} (Z = 71) have zero spin momentum (Table S1). The extra absorption features in the NIR region associated with the $S_0 \rightarrow T_n$ transition are only observed in the blends with non-zero spin, while no features can be observed for the Y^{3+} and Lu^{3+} blends despite the high atomic mass of Lu^{3+} (fig. S5 and S6). This result shows that spin-orbit coupling is not responsible for the effect.

To understand the nature of the coupling between the molecular triplet exciton and the lanthanide ions, we perform highly-correlated wavefunction calculations at the complete active space self-consistent field (CASSCF) level (without and with spin-orbit coupling, SOC, interactions) for the $NaGdF_4$:Yb-tetracene systems. Full details of calculations are presented in the SM (figs. S7-S10). The calculations confirm the formation of coupled excited states at an energy close to those predicted at the same level of theory for a triplet on a tetracene molecule, namely at ~ 1.2 eV for the larger model considered (see SM for details). A simplified picture for the relevant electronic excitations of the models investigated is shown in Figure 1D. The inclusion of SOC lifts the degeneracy of the f orbitals and results in an electronic transition from the J = 7/2 ground state to the J = 5/2 excited state of the Yb-doped

cluster at ~ 1.2 eV, in excellent agreement with experiment. When the lanthanide center is brought into interaction with tetracene, the f-f electronic states further split into multiple components as a result of partial hybridization. At the same level of theory, the tetracene triplet (lower state on the T_1 band in Figure 1D) is predicted at about the same energy as the Yb excitation, again in line with the spectroscopic data. The upper-lying electronic states in that band, at 2.2-2.6 eV, correspond to triplet-lanthanide states involving a superposition of the tetracene triplet and Yb f-f excitations. Based on these calculations we propose that the proximity of the organic molecules to the lanthanide ions permits exchange coupling of spins between the molecule and lanthanide. This enables photon absorption to directly generate triplet states, $S_0 \rightarrow T_n$, as the creation of the triplet on the molecule is accompanied by a spin flip on the lanthanide, resulting in zero net spin change for the combined system, as illustrated in Figure 1E.

To better understand the effect of this exchange coupling on the dynamics of excitations we turn to pump-probe spectroscopy. The solid-state blends of the organics with lanthanide nanoparticles form films that are unsuitable for pump-probe spectroscopy due to scattering from the nanoparticles. Instead we use CPPOA molecules directly attached to lanthanide nanoparticles in the solution phase as a model system, illustrated in Figure 2A. We began by attaching CPPOA to $NaYF_4/NaGdF_4$ core/shell particles and found that the system showed a pronounced sub-gap absorption as compared with the pristine CPPOA molecules (fig. S11A), suggesting a strong exchange interaction between the molecule and the lanthanides. We excite the CPPOA at 355 nm to create singlet excitons (S_1) on the molecules and subsequently probe the evolution of the spectral features as a function of time (see SM for full details). We note that the Gd^{3+} has no absorption features in this region and thus the entire response arises from the excited state features of CPPOA. As shown in Figure 2B, the S_1 state of CPPOA in the

coupled system is found to decay with an 82 ps time constant, concomitant with the rise of the triplet excitons (T_1, rise constant of 96 ps). This shows that the photogenerated singlet of CPPOA attached to $NaYF_4/NaGdF_4$ undergoes rapid intersystem crossing (ISC). In contrast, the singlet on the pristine CPPOA shows a decay constant of 12.9 ns with a concomitant triplet rise over 18.4 ns. Thus, the presence of the Gd^{3+}-based nanoparticles increases the rate of ISC by three orders of magnitude (Fig. 2C). To probe this further, we attached CPPOA to a series of $NaYF_4/NaLnF_4$ core/shell particles with different lanthanide ions in the shell and measured the triplet generation rate. As shown in Figure 2D, we observe an enhanced triplet rise rate when CPPOA molecules are on the nanoparticles containing lanthanides with unpaired 4f electrons (Tb^{3+}, Eu^{3+}, Gd^{3+} and Yb^{3+}). However, the nanoparticles with no unpaired spins (Y^{3+} and Lu^{3+}) show no obvious enhancement in ISC (Table S1). For the Eu^{3+}-doped nanoparticles we measured a triplet rise time of 9.3 ps, which was 1978 times faster than that of pristine CPPOA molecules. The ISC efficiency is estimated to be 99.4 %, based on the singlet lifetime quenching. It is thus clear that in addition to turning $S_0 \rightarrow T_n$ transitions bright, the exchange-coupling between the CPPOA and the lanthanide nanoparticles also yields highly efficient ISC (see figs. S12-S33 and SM for full details).

It can be seen in Figure 2D that the fast rise of the T_1 state for Tb^{3+} and Eu^{3+} containing nanoparticles is accompanied by a quick decay of the T_1 state (883 ps for Eu^{3+} and 7.66 ns for Tb^{3+}). This decay is caused by the transfer of the T_1 state from the CPPOA to the $^5D_0$ and $^5D_4$ transitions in the Eu^{3+} and Tb^{3+} respectively, as illustrated in Figure 3A. Based on the quenching of the triplet lifetime, we calculate that the quantum efficiency of triplet energy transfer from CPPOA to nanoparticles exceeds 99 %. This near quantitative triplet transfer to the lanthanide nanoparticles gives rises to bright luminescence from the lanthanide ions upon excitation of the coupled systems at 365 nm, as shown in Figure 3B. The

corresponding unmodified nanoparticles show a very weak emission in comparison (fig. S11B). Here, the molecule with its large absorption cross-section acts as an efficient antenna for capturing photons and generating singlet excitons. The exchange coupling then allows rapid conversion of the singlet into triplet excitons which can then transfer energy to the lanthanide ions.

This luminescent harvesting of triplet excitons is not restricted to the triplets generated by ISC on the surface of the nanoparticles. Returning to the blend films described in Figure 1, we note that tetracene and rubrene are both well-known singlet fission materials (*16, 17*), where the photogenerated singlet excitons rapidly and efficiently convert to a pair of triplet excitons. As shown in Figure 3C, when the $NaGdF_4$:Yb-tetracene blend film is excited at 405 nm, we see a strong quenching of the characteristic visible emission from tetracene (which arises mostly from triplet-triplet annihilation (TTA) of the fission generated triplets) in favour of a NIR emission located at 950-1100 nm, which can be assigned to the $^2F_{5/2} \rightarrow {}^2F_{7/2}$ transition of Yb^{3+}. As the $NaGdF_4$:Yb nanoparticles do not have any absorption at this excitation energy (fig. S3), photoexcitation leads to the formation of excited states on tetracene and the emission from Yb^{3+} must arise from energy transfer from tetracene to Yb^{3+}. The emission of Yb^{3+} in the blend is found to be sensitive to the presence of oxygen, as significant quenching in the Yb^{3+} emission intensity occurs when the blend is exposed to air (fig. S34), suggesting a triplet-mediated process. Magnetic field dependent photoluminescence (MPL) measurements show that, on the application of a magnetic field of a few hundred mT, the visible emission (arising from the tetracene) increases (fig. S39), as would be expected for the singlet fission process. In contrast, the emission from the Yb^{3+} decreases (fig. S41), proving that it arises via transfer of the fission-generated triplets to the $^2F_{5/2} \rightarrow {}^2F_{7/2}$ transition of Yb^{3+}.

In comparison, the emission intensity of Yb^{3+} is much weaker than that of the singlet emission of rubrene for the $NaGdF_4$:Yb-rubrene blend (Fig. 3C). This is consistent with the energetically unfavourable nature of the triplet-to-lanthanide energy transfer from rubrene (rubrene T_1 ~1.14 eV, tetracene T_1 ~1.25 eV, vs 1.25eV for the $^2F_{5/2} \rightarrow {}^2F_{7/2}$ transition of Yb^{3+}). Based on theoretical calculations (see SM for full details), we propose that the energy transfer process is mediated by (virtual) charge-transfer (CT) excitations involving an electron transfer from the excited molecule to the lanthanide (thus now becoming a closed shell system), whose energies are predicted to be close to the bottom of the T_1 band. This is shown in Figure 3D and supported by a careful analysis of the many-body electronic wavefunctions in the lowest adiabatic singlet and triplet excited states that comprise small admixtures (0.1-1%) from CT excitations. These results explain the efficient sensitization of lanthanide luminescence with organic molecules (*18*) and show that it is mediated by triplet excitons, providing a way to luminescently harvest otherwise dark triplet excitons.

Figure 4A shows the photoluminescence spectra of the $NaGdF_4$:Yb-rubrene and $NaGdF_4$:Yb-tetracene blend when excited by a 980-nm laser diode. The spectra corresponding to the singlet emission from both tetracene and rubrene were obtained, consistent with upconversion of absorbed energy. This upconverted emission was bright and clearly observable even with the room lights on (fig. S35) and was found to have a quadratic dependence on the excitation power at low excitation fluence, followed by a slope change from 2 to 1 at higher excitation density (figs. S36 and S47). This phenomenon is analogous to the power dependence reported in conventional triplet-triplet annihilation (TTA, ref *19-21*) upconversion and energy transfer upconversion (ETU, ref *22*) processes in organic and lanthanide systems (*23, 24*), respectively. At first glance, these results would appear similar to recent work in organic/quantum dots (QDs) systems, where upconversion is obtained via excitation

of QDs, such as PbS (*25*), PbSe (*26*) and CdSe (*2*), followed by energy transfer from the QDs into the triplet states of molecules and TTA within the organic materials. However, as we argue below, the upconversion mechanism seen here has a completely different origin and is based on the fusion of molecular triplet energy with the lanthanide energy to give a molecular singlet state (Fig. 4B).

The $NaGdF_4$:Yb-rubrene blend has a broad absorption in the NIR wavelength region (Figure 1B), not just at 980 nm which is the peak absorption of Yb^{3+}. We excited the sample over a broad range of wavelengths in the NIR (850-1020 nm) and obtained upconverted emission at all excitation wavelengths (fig. S37), suggesting that the exchange coupling of the molecular triplet exciton and lanthanide and resulting transitions mediate the upconversion process (Fig. 1E), rather than the conventional TTA process in organic molecules after triplet transfer from photoexcited Yb^{3+}-doped nanoparticles under NIR irradiation. To further investigate the upconversion mechanism, we prepared a series of blends with varying concentration ratios of $NaGdF_4$:Yb and rubrene or tetracene. As shown in Figure 4C, the main emission peak shifts from 540 (2.29 eV) to 480 nm (2.58 eV) for the $NaGdF_4$:Yb-tetracene blends, when the tetracene: nanoparticle concentration ratio is changed from 10:1 to 1:100 (data for rubrene blends are shown in fig. S38). Interestingly, an emission characteristic of the single tetracene molecule (*27*) is obtained when the concentration of tetracene was diluted to as low as 1 molecule to 100 nanoparticles. This upconverted emission is recorded at room temperature at moderate excitation density (< 10 W/cm^2). This is in stark contrast to conventional two-photon absorption methods for generating anti-Stokes emission from single molecules, which require a significantly higher excitation density (> 10^6 W/cm^2). Conventional TTA upconversion proceeds via bimolecular triplet-triplet states (*28, 29*) and would not allow us to obtain the single molecular emission of tetracene, as the emission would be shifted to lower energies due to excitonic coupling, as happens

when we increase the tetracene concentration in the blend films. This again suggests that the upconverted emission is produced by a different process. MPL studies show no change in upconverted emission under applied magnetic field (fig. S40), confirming that the upconversion process is not mediated by TTA (see fig. S43 and SM for full details).

Interestingly, given that the singlet energy of molecular tetracene (for a single molecule) is higher (2.62 eV; figs. S42 and S44) than the total energy contained in two excitation photons (1.25 eV × 2 = 2.50 eV), this new mechanism enables us to obtain endothermic upconversion, which has not been achieved by other upconversion approaches. To investigate this endothermic upconversion process further, we performed temperature dependent upconversion measurements. As shown in Figure 4D, the upconversion emission intensity for the 1:100 film keeps increasing down to 80 K, presumably due to the suppression of non-radiative loss channels at low temperature. However, further lowering the temperature results in a decrease of the upconversion emission. We note that the downconversion luminescence of the same sample under 405 nm excitation increases monotonically as the temperature drops, and the integrated PL intensity increases by more than 12 times between room temperature and 20 K (fig. S45). More interestingly, we find that the upconversion emission continuously redshifts as the temperature is lowered. The peak emission of tetracene shifts by a maximum of ~ 35 meV when the temperature is reduced from 297 to 10 K (fig. S46). Taken together, these results show that the upconversion of $NaGdF_4$:Yb-tetracene (with 1:100 concentration) is thermally activated.

We also measured the absolute upconversion photoluminescence quantum efficiency (PLQE) of the $NaGdF_4$:Yb-rubrene blend as a function of irradiance power density. We applied a modified integrating sphere method using a continuous wave 980 nm diode laser as the excitation source (*30*). At room

temperature, more than 1 % PLQE can be obtained with moderate excitation of > 16 W/cm^2. A maximum PLQE value of 1.9 ± 0.5 % is reached at an irradiance power density of 75 W/cm^2 (Fig. 4E). Note that the singlet PLQE of rubrene in the blend was measured to be 20 ± 2.1 %. This suggests a maximum singlet yield of ~ 10 % per absorbed NIR photon for the $NaGdF_4$:Yb-rubrene. Furthermore, as shown in the inset of Figure 4E, the upconversion PLQE monotonously increases as the temperature goes down due to the reduction of the non-radiative energy loss pathways from both of the organic and the lanthanide nanocrystals. A maximum PLQE value of 16.2 ± 3.4 % is attained at 10 K (fig. S48). Given the fact that two lower-energy photons are converted to one higher-energy photon during the upconversion process, our system has thus converted ~ 32 % of the absorbed photons. These values are high for solid-state systems, for instance, higher than the maximum absolute quantum efficiency obtained in solid-state PbS-sensitized triplet-triplet annihilation upconversion using similar organic molecules (*31*).

It is clear that the upconversion does not arise from TTA. We propose that NIR excitation leads to the direct population of triplet states due to the coupling between molecular triplet and the lanthanide ions at or near the surface. The triplet then combines with excitation in the matched 4f energy levels of lanthanides, upconverting the two low-energy states to the high-energy singlet states in the organic molecules (Fig. 4B). In analogy with the corresponding process in molecular crystals, our calculations suggest that the fusion process is mediated by the same (virtual) CT that steer energy transfer from the organic to the lanthanide. The proposed superexchange mechanism is schematized in Figure 4F, where the CT1 and CT2 states involve the ground state and the excited state of the tetracene cation, respectively.

In comparison with the conventional lanthanide or TTA based upconversion, a key feature of the lanthanide-triplet excitation fusion approach demonstrated here is that the excitation energy can be directly amassed in both organic and inorganic components without the need for a sensitization step. Therefore, energy loss during the sensitization process can be effectively reduced to zero. In addition, unlike organic/QDs systems, where the QDs have large absorption cross-sections at high energies where the upconverted emission is generated, the lanthanide-doped nanoparticles have no absorption at higher energies, eliminating the problem of reabsorption. Furthermore, because of the spin-exchange coupling between the organic and the lanthanide, normal spin statistical limitations that apply to conventional TTA are irrelevant to lanthanide-triplet upconversion.

In conclusion, we have demonstrated that very surprisingly it is possible to electronically and spin couple conventional molecular systems to lanthanide-doped inorganic nanoparticles. The combination of exchange coupling of spins and CT type interactions enables the direct photogeneration of triplets from the ground state, rapid (sub-10 ps) and efficient (> 99 %) ISC from the S_1 to T_1 state, triplet energy transfer to lanthanide ions with near unity efficiency followed by photon emission, and a new lanthanide-triplet exciton fusion process that gives highly efficient upconversion and even endothermic upconversion. Here, triplet sensitization can be achieved with no energy loss penalty, in comparison to the energy losses inherent in triplet sensitization via ISC in conventional systems. In addition, unlike the use of quantum dots to generate triplet states, lanthanide-doped nanoparticles are highly stable in a variety of solvents (including water) and solid-state media and do not undergo photobleaching. These results establish a new methodology to control and manipulate triplet excitons, one that potentially offers more opportunities than heavy metal based spin-orbit coupling or the control of singlet-triplet energy splitting, which are the two dominant paradigms today. We thus expect these results to enable

new avenues for triplet sensitization, photocatalysis, optoelectronics, sensing, and photon frequency conversion driven by optically bright triplet excitons.

References

1. H. Uoyama, K. Goushi, K. Shizu, H. Nomura, C. Adachi, *Nature* **492,** 234-238 (2012).
2. C. Mongin, S. Garakyaraghi, N. Razgoniaeva, M. Zamkov, F. N. Castellano, *Science* **351**, 369-372 (2016).
3. M. A. Baldo *et al., Nature* **395,** 151-154 (1998).
4. F. Auzel, *Chem. Rev.* **104**, 139-174 (2004).
5. T. F. Schulze, T. W. Schmidt, *Energy Environ. Sci.* **8**, 103-125 (2015).
6. B. D. Ravetz *et al.*, *Nature* **565**, 343-346 (2019).
7. A. Kohler, H. Bassler, *Mater. Sci. Eng. R* **66**, 71-109 (2009).
8. T. J. Penfold, E. Gindensperger, C. Daniel, C. M. Marian, *Chem. Rev.* **118**, 6975-7025 (2018).
9. M. B. Smith, J. Michl, *Chem. Rev.* **110**, 6891-6936 (2010).
10. S. Lamansky *et al., J. Am. Chem. Soc.* **123**, 4304-4312 (2001).
11. O. Bolton, K. Lee, H. J. Kim, K. Y. Lin, J. Kim, *Nat. Chem.* **3**, 205-210 (2011).
12. S. I. Klink, H. Kerizer, F. C. J. M. van Veggel, *Angew. Chem. Int. Ed.* **39**, 4319-4321 (2000).
13. A. Tiberghien, G. Delacote, *Chem. Phys. Lett.* **8**, 88-90 (1971).
14. S. Tao *et al., Phys. Rev. B* **83**, 075204 (2011).
15. C. K. Yong *et al., Nat. Commun.* **8**, 15953 (2017).
16. P. M. Zimmerman, F. Bell, D. Casanova, M. Head-Gordon, *J. Am. Chem. Soc.* **133**, 19944-19952 (2011).
17. L. Ma *et al*., *Phys. Chem. Chem. Phys.* **14**, 8307-8312 (2012).
18. D. J. Garfield *et al., Nat. Photon.* **12**, 402-407 (2018).
19. M. Wu *et al., Nat. Photon.* **10**, 31-34 (2016).
20. J. Zhao, S. Ji, H. Guo, *RSC Adv.* **1**, 937-950 (2011).
21. T. N. Singh-Rachford, F. N. Castellano, *Coord. Chem. Rev.* **254**, 2560-2573 (2010).
22. M. Haase, H. Schäfer, *Angew. Chem. Int. Ed.* **50**, 5808-5829 (2011).

23. M. Pollnau, D. R. Gamelin, S. R. Lüthi, H. U. Güdel, M. P. Hehlen, *Phys. Rev. B* **61**, 3337-3346 (2000).
24. A. Monguzzi, J. Mezyk, F. Scotognella, R. Tubino, F. Meinardi, *Phys. Rev. B* **78**, 78, 195112 (2008).
25. N. J. Thompson *et al., Nat. Mater.* **13**, 1039-1043 (2014).
26. M. Tabachnyk *et al., Nat. Mater.* **13**, 1033-1038 (2014).
27. J. J. Burdett, A. M. Müller, D. Gosztola, C. J. Bardeen, *J. Chem. Phys.* **133**, 144506 (2010).
28. J. F. Suyver *et al.*, *Opt. Mater.* **27**, 1111-1130 (2005).
29. S. Amemori, Y. Sasaki, N. Yanai, N. Kimizuka, *J. Am. Chem. Soc.* **138**, 8702-8705 (2016).
30. J. C. de Mello, H. F. Wittmannn, R. H. Friend, *Adv. Mater.* **9**, 230-232 (1997).
31. L. Nienhaus *et al.*, *ACS Nano* **11**, 7848-7857 (2017).

Acknowledgements

We acknowledge support from the Engineering and Physical Sciences Research Council (EPSRC), European Research Council (ERC) and the Winton Programme for the Physics of Sustainability, the Singapore Ministry of Education (Grant R143000A31112), Agency for Science, Technology and Research (Grant R143000A34305), and National Research Foundation, Prime Minister's Office, Singapore under its Competitive Research Program (CRP Award No. NRF-CRP15-2015-03). R. D. acknowledges supports from National Natural Science Foundation of China (51872256) and Zhejiang Provincial Natural Science Foundation of China (LR19B010002). This project has received funding from the European Union's Horizon 2020 research and innovation programme under the Marie Skłodowska-Curie grant agreement No 797619 (TET-Lanthanide project), No 748042 (MILORD project) and No 646176 (EXTMOS project). Computational resources have been provided by the Consortium des Équipements de Calcul Intensif (CÉCI), funded by the Fonds de la Recherche Scientifique de Belgique (F.R.S.-FNRS) under Grant No. 2.5020.11 as well as the Tier-1 supercomputer of the Fédération Wallonie-Bruxelles, infrastructure funded by the Walloon Region under the grant agreement n1117545. D.B. is a FNRS Research Director.

Supplementary Materials

Materials and Methods
Supplementary Text
Figs. S1 to S48
Table S1

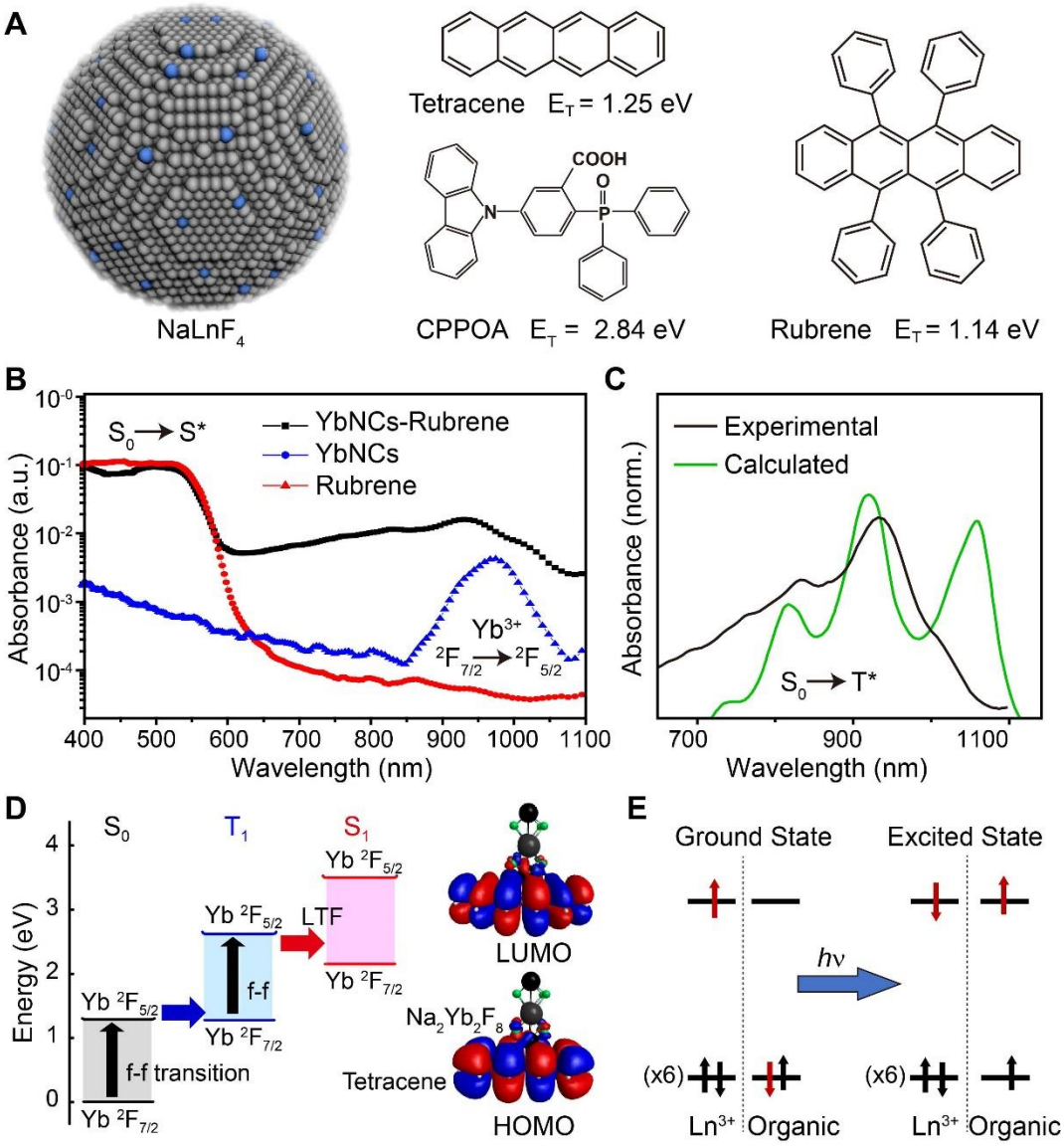

Fig. 1. Lanthanide nanocrystal-coupled triplet excitation. (**A**) Schematic illustration of a lanthanide-doped nanocrystal ($NaLnF_4$) and the organic molecules in our study. (**B**) Comparison of the PDS spectra of $NaGdF_4$:Yb (YbNCs)-rubrene with pristine rubrene and neat YbNCs film. (**C**) The nanocrystal-organic blend features a broadband absorption from 700 to 1100 nm which matches the calculated direct transition from the ground singlet state (S_0) to the triplet state (T*). (**D**) Schematic state energy diagram and wavefunction hybridization as computed for a complex between a tetracene molecule and a $Na_2Yb_2F_8$ nanocluster at the CASSCF(SOC)/CASPT2 level with a distance of 2.5 Å. S_0, T_1, and S_1 correspond to electronic excitations where the tetracene molecule is in its singlet ground state, lowest triplet excited state, and lowest singlet excited state, respectively. The bottom (top) states refer to the Yb^{3+} being in the $^2F_{7/2}$ ($^2F_{5/2}$) state. (**E**) Scheme showing the spin-allowed optical transition to form triplet excitons directly from the ground state. The two spin flips are illustrated by red colors.

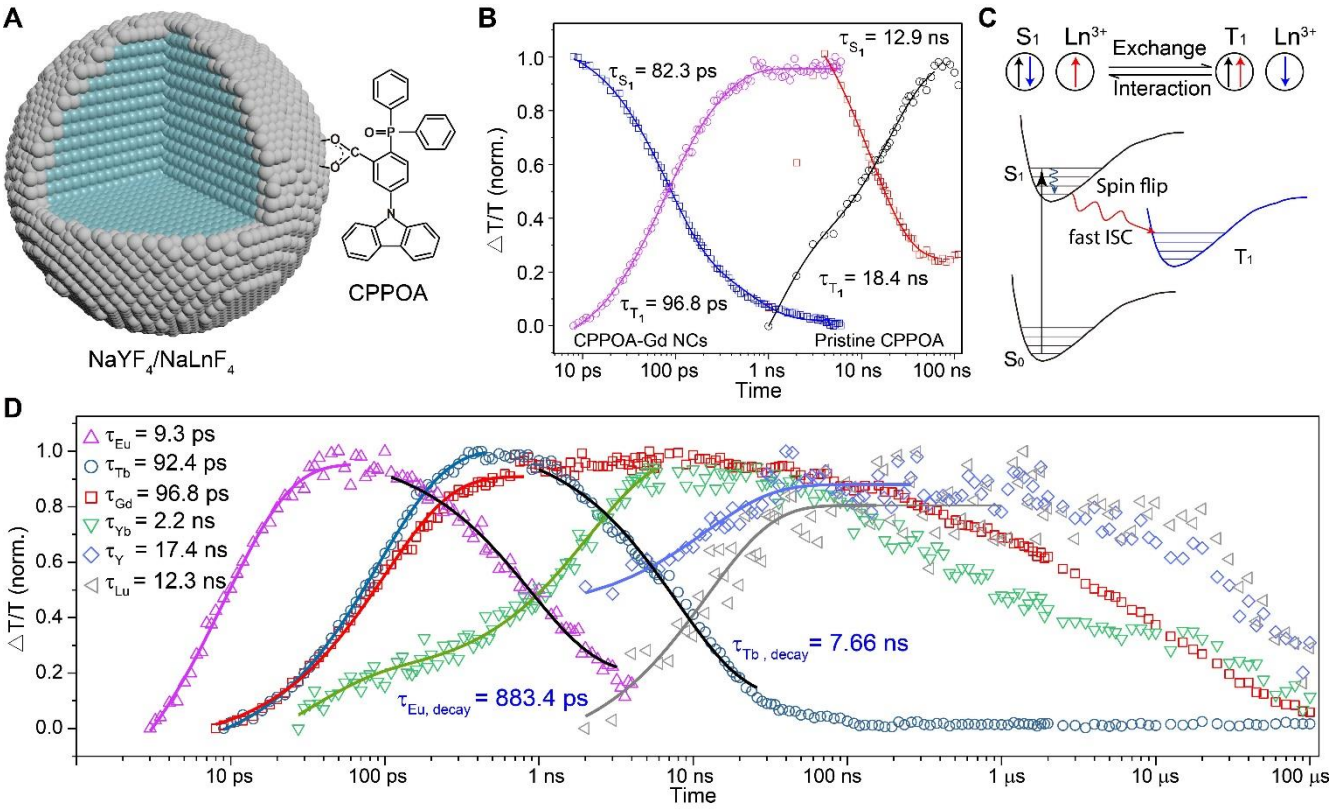

Fig. 2. Ultrafast pump-probe spectroscopic investigation of organic molecules coupled to a lanthanide-doped nanoparticle. (**A**) Schematic illustration of an $NaYF_4/NaLnF_4$ core/shell nanoparticle modified with CPPOA. (**B**) The extracted kinetics showing the singlet (S_1) decay and triplet (T_1) rise of a solution containing pristine CPPOA molecules and a solution of CPPOA-modified $NaYF_4$@$NaGdF_4$ nanoparticles. The singlet lifetime decreases from 12.9 ns in the pristine CPPOA to 82.3 ps in CPPOA-modified $NaYF_4/NaGdF_4$ indicating greatly enhanced intersystem crossing (ISC). (**C**) Proposed mechanism showing that a spin flip of the electron due to the exchange interaction between the lanthanides and the organic can accelerate the ISC from the singlet to triplet states of the molecule. (**D**) Kinetics of triplet generation and decay in the CPPOA molecules attached to different types of core/shell nanoparticles. The compositions of the core-shell nanoparticles are $NaYF_4/NaEuF_4$, $NaYF_4/NaGdF_4$, $NaYF_4/NaTbF_4$, $NaYF_4/NaYbF_4$, $NaYF_4/NaLuF_4$, and $NaYF_4/NaYF_4$. For lanthanides with unpaired 4f electrons (Tb^{3+}, Eu^{3+}, Gd^{3+} and Yb^{3+}) enhanced ISC is seen, while those with no unpaired spins (Y^{3+} and Lu^{3+}) show no obvious enhancement in ISC. In addition, an enhanced triplet decay (7.66 ns and 883 ps) of CPPOA on the nanoparticles containing Tb^{3+} or Eu^{3+} shows via transfer triplet energy transfer to the lanthanide ions.

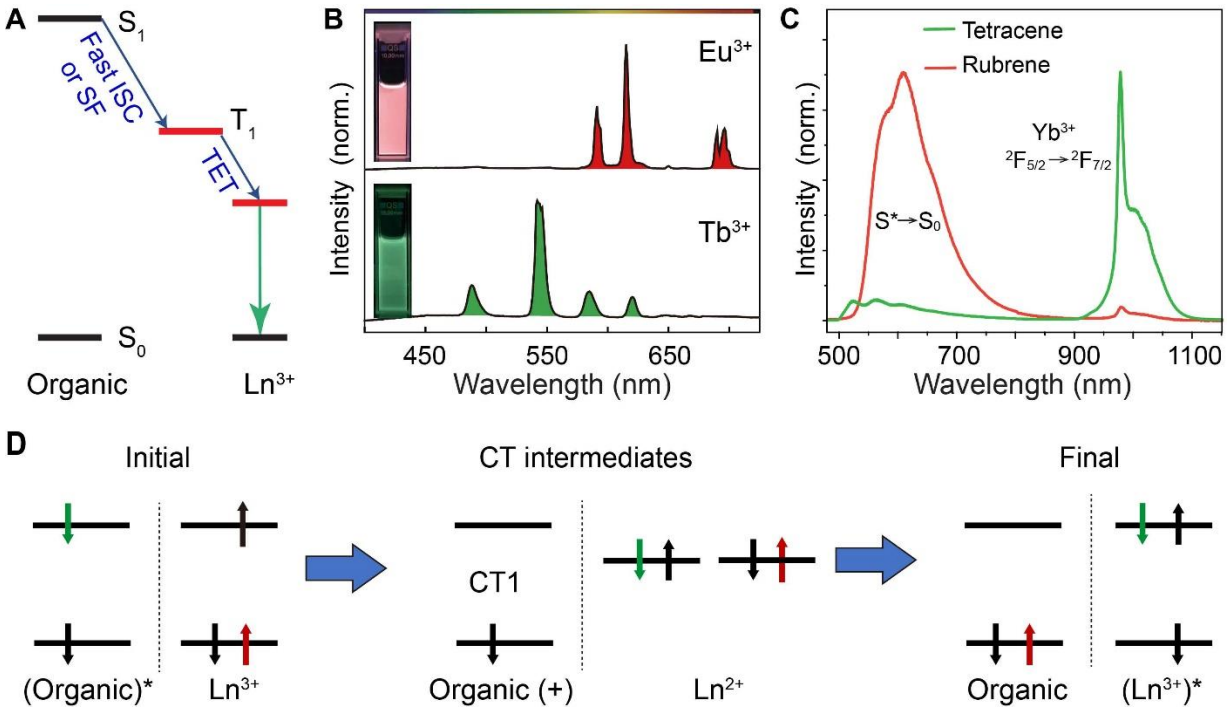

Fig. 3. Triplet energy transfer from molecules to nanoparticles. (A) Simplified energy diagram showing the triplet energy transfer (TET) from molecular triplet state to lanthanide emitters (Ln^{3+}) following a fast intersystem crossing (ISC) or singlet fission (SF) process. **(B)** Photoluminescence spectra and corresponding luminescence photos of colloidal solutions containing CPPOA-modified $NaYF_4$/$NaTbF_4$ and $NaYF_4$/$NaEuF_4$ nanoparticles under excitation at 365 nm. (**C**) Photoluminescence spectra of $NaGdF_4$:Yb-tetracene and $NaGdF_4$:Yb-tetracene blend films excited at 405 nm. Luminescence arises from the transfer of triplet excitons generated via fission to the $^2F_{5/2}\rightarrow{}^2F_{7/2}$ transition of Yb^{3+}. The process is inefficient in rubrene due to its triplet energy being lower than the $^2F_{5/2}\rightarrow{}^2F_{7/2}$ transition of Yb^{3+} (1.14 vs 1.25 eV). (**D**) Schematic of charge transfer (CT)-mediated triplet energy transfer processes.

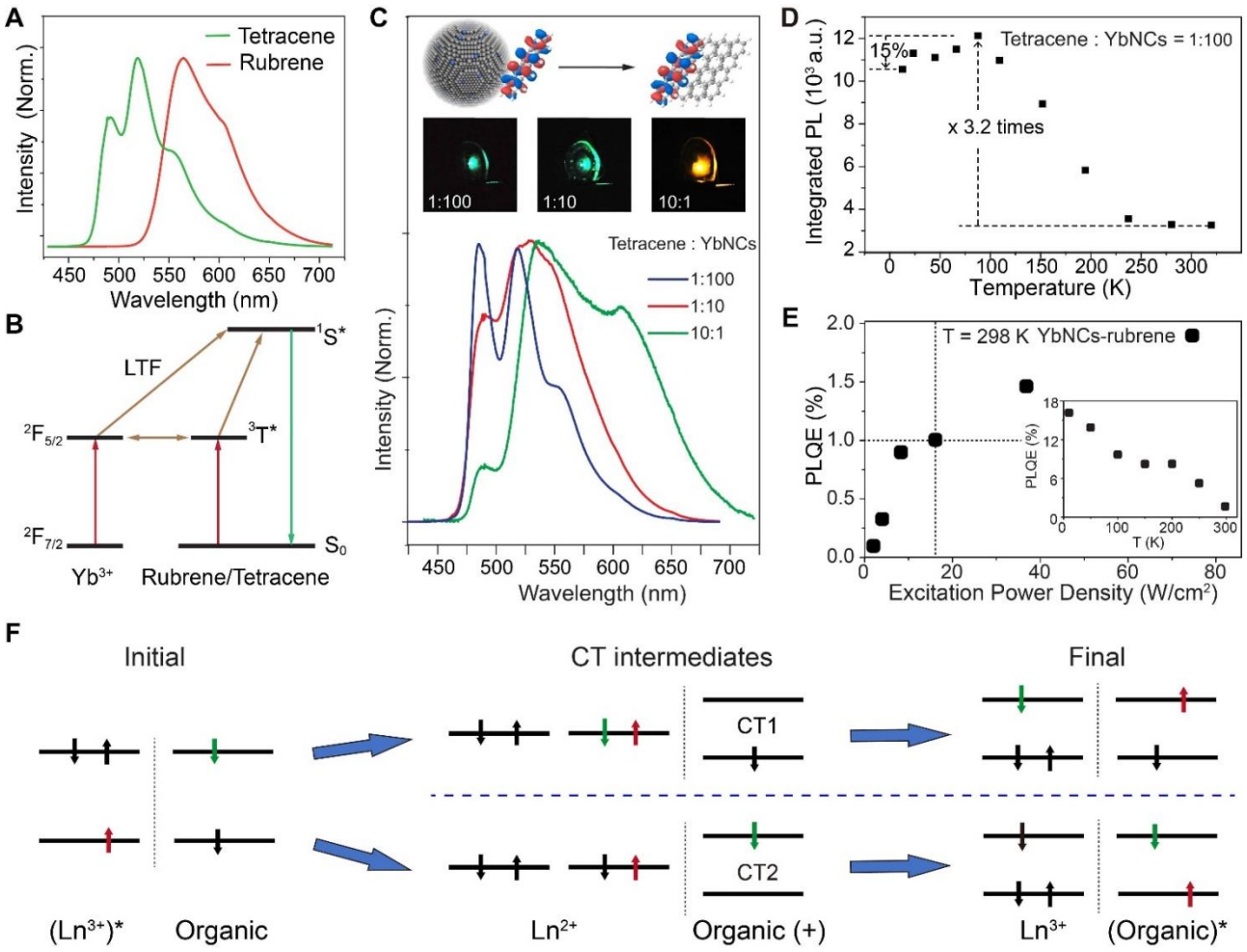

Fig. 4. (**A**) Photoluminescence spectra of $NaGdF_4$:Yb-tetracene and $NaGdF_4$:Yb-Rubrene blend films excited at 980 nm, showing upconverted emission arising from the singlet state of the organics. (**B**) Proposed lanthanide-triplet exciton fusion (LTF) upconversion process. Upconversion by LTF involves a coupled lanthanide-organic pairs, which absorbs and subsequently converts low-energy photons to high-energy emission. (**C**) Upconversion spectra and corresponding emission photographs of $NaGdF_4$:Yb-tetracene blend films with varying nanocrystal-to-tetracene ratios in the films. (**D**) The plot of the temperature dependent upconversion emission of the $NaGdF_4$:Yb-tetracene blend films (tetracene: $NaGdF_4$:Yb = 1:100) blend integrated from 475 to 650 nm. (**E**) The absolute quantum efficiency of the $NaGdF_4$:Yb-rubrene blend measured as a function of excitation power density. (Inset) Temperature dependent quantum efficiency of the same sample under excitation of 980 nm for a power density of 76 W/cm^2. (**F**) Schematic of lanthanide-triplet excitation fusion upconversion processes. CT1 and CT2 involve the ground state and the excited state of the organic cation, respectively.